A&A 593, L12 (2016)
DOI: 10.1051/0004-6361/201628899

Astronomy & Astrophysics

Letter to the Editor

The first CO^+ image

I. Probing the HI/H_2 layer around the ultracompact HII region Mon R2

S. P. Treviño-Morales[1,2], A. Fuente[2], Á. Sánchez-Monge[3], P. Pilleri[4,5], J. R. Goicoechea[1], V. Ossenkopf-Okada[3], E. Roueff[5], J. R. Rizzo[6], M. Gerin[5], O. Berné[4,7], J. Cernicharo[1], M. Gónzalez-García[8], C. Kramer[9], S. García-Burillo[2], and J. Pety[10]

[1] Instituto de Ciencia de Materiales de Madrid, Sor Juana Inés de la Cruz 3, 28049 Cantoblanco, Madrid, Spain
e-mail: trevino@iram.es
[2] Observatorio Astronómico Nacional, Apdo. 112, 28803 Alcalá de Henares Madrid, Spain
[3] I. Physikalisches Institut, Universität zu Köln, Zülpicher Str. 77, 50937 Köln, Germany
[4] CNRS; IRAP; 9 Av. colonel Roche, BP 44346, 31028 Toulouse Cedex 4, France
[5] LERMA, Observatoire de Paris, PSL Research University, CNRS, UMR 8112, Place Janssen, 92190 Meudon Cedex, France
[6] Centro de Astrobiología, 28850 Torrejón de Ardoz, Spain
[7] Université de Toulouse, UPS-OMP, IRAP, 31000 Toulouse, France
[8] Instituto de Astrofísica de Andalucía, CSIC, 18008 Granada, Spain
[9] Instituto de Radioastronomía Milimétrica, Ave. Divina Pastora, 7, Local 20 18012 Granada, Spain
[10] Institut de Radioastronomie Millimétrique, 300 rue de la Piscine, 38406 Saint-Martin d'Hères, France

Received 11 May 2016 / Accepted 8 August 2016

ABSTRACT

The CO^+ reactive ion is thought to be a tracer of the boundary between a HII region and the hot molecular gas. In this study, we present the spatial distribution of the CO^+ rotational emission toward the Mon R2 star-forming region. The CO^+ emission presents a clumpy ring-like morphology, arising from a narrow dense layer around the HII region. We compared the CO^+ distribution with other species present in photon-dominated regions (PDR), such as [CII] 158 μm, H_2 S(3) rotational line at 9.3 μm, polycyclic aromatic hydrocarbons (PAHs), and HCO^+. We find that the CO^+ emission is spatially coincident with the PAHs and [CII] emission. This confirms that the CO^+ emission arises from a narrow dense layer of the HI/H_2 interface. We determined the CO^+ fractional abundance relative to C^+ toward three positions. The abundances range from 0.1 to 1.9×10^{-10} and are in good agreement with the previous chemical model, which predicts that the production of CO^+ in PDRs only occurs in dense regions with high UV fields. The CO^+ linewidth is larger than those found in molecular gas tracers, and their central velocity are blueshifted with respect to the molecular gas velocity. We interpret this as a hint that the CO^+ is probing photoevaporating clump surfaces.

Key words. astrochemistry – photon-dominated region – HII regions – radio lines: ISM

1. Introduction

Reactive ions are destroyed in almost every collision with H and H_2 and recombine rapidly with e^-. These compounds present enhanced abundances toward the hot layers of photon-dominated regions (PDRs), where the far ultraviolet (FUV) field is only partially attenuated and maintains high abundances of the parent species C^+ and S^+ (Sternberg & Dalgarno 1995). In particular, Sternberg & Dalgarno (1995) predict a high CO^+ abundance at the HI/H_2 interface ($A_V \approx 1$ mag) of dense PDRs, where it is mainly produced by the $C^+ + OH \rightarrow CO^+ + H$ reaction. So far, the CO^+ ion has been detected in several PDRs, such as the M17SW, Orion Bar, NGC 7027, NGC 7023 (Latter et al. 1993; Stoerzer et al. 1995; Fuente & Martín-Pintado 1997; Fuente et al. 2003), G29.96, MonR2 (Rizzo et al. 2003) and S140 (Savage & Ziurys 2004). However, all of these detections were obtained after long integrations toward a single position and they lack information on spatial distribution.

The Mon R2 star-forming region, located at 830 pc (Herbst & Racine 1976), contains an ultracompact (UC) HII region surrounded by a series of PDRs with different physical conditions (Pilleri et al. 2013; Treviño-Morales et al. 2014). The main PDR, corresponding to IRS 1 (hereafter IF), is irradiated by a high UV field of $G_0 > 10^5$ (in units of the Habing flux; Habing 1968), and presents high densities ($>10^5$ cm^{-3}) and kinetic temperatures ($T_k \approx 600$ K; Berné et al. 2009). A second PDR, associated with the molecular peak MP2, is detected 40″ north from IF, and shows chemical properties similar to those found in low- to mid-UV irradiated PDRs (Ginard et al. 2012). Because of its proximity and physical conditions, Mon R2 turns to be an excellent candidate to study the HI/H_2 interface. CO^+ is thought to be a good PDR tracer, and its distribution is potentially an excellent diagnostic tool to learn about the physical structure of these regions.

In this paper, we present a study of the CO^+ ($J = 2-1$) transition line toward Mon R2 and compare its spatial distribution with *Spitzer* data reported by Berné et al. (2009), *Herschel* data from Pilleri et al. (2012) and Ossenkopf et al. (2013), and the HCO^+ and $H^{13}CO^+$ molecules from Treviño-Morales et al. (2014).

2. Observations and data reduction

We observed $2' \times 2'$ maps of CO^+ transition lines ($J = 2-1$ at 235.380 GHz, 235.789 GHz and 236.062 GHz) using the IRAM 30 m telescope (Pico Veleta, Spain). The observations were performed using the EMIR receiver with the fast Fourier transform

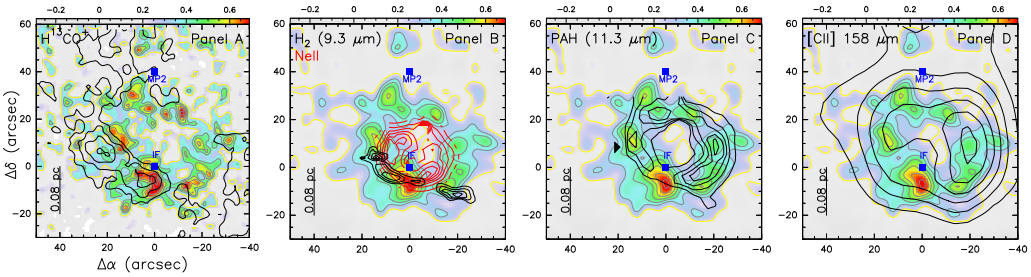

Fig. 1. Integrated emission (in K km s^{-1}) of the CO$^+$ line with the original (11″, panel **A**)) and smoothed (16″, panels **B)** to **D**)) angular resolution. In panels **A)** to **D)**, the gray contour levels range from 40% to 100% in steps of 10% of the intensity peak, where the lower contour level corresponds to a $S/N = 5\sigma$. The yellow contour indicates the 3σ emission. The blue squares indicate the IF and MP2 positions, where IF corresponds to α(J2000) = 06h07m46.2s, δ(J2000) = −06°23′08.3″. panel **A)** shows the H^{13}CO$^+$ (3−2) emission (black contours) tracing the molecular gas (Treviño-Morales et al. 2014). Panel **B)** shows the [Ne II] emission (red contours) tracing the HII region and the emission of the H_2 S(3) rotational line at 9.7 μm (black contours). Black contours in panel **C)** show the PAHs (11.3 μm) emission. Panel **D)** shows the [CII] emission at 158 μm (black contours; Pilleri et al. 2014). The *Spitzer* data are explained in Berné et al. (2009).

spectrometer (FTS) at 200 kHz of resolution. Throughout this paper, we use the main-beam brightness temperature (T_{MB}) as intensity scale. The data were reduced using standard procedures with the CLASS/GILDAS package (Pety et al. 2005). The three lines were detected, but only the 236.0625 GHz has sufficient signal-to-noise ratio (S/N) for good imaging. In order to improve the S/N, we smoothed the native observation to an angular resolution of 16″ (see Fig. 1) and to a spectral resolution of 1 km s^{-1}. In the final data cube, CO$^+$ has linewidths of 6–8 km s^{-1} and intensity peaks of 60−200 mK (with rms ∼ 20 mK). The main CO$^+$ line is located close to a bright $^{13}CH_3OH$ line (at 236.0628 GHz). However, we dismiss the idea of a possible blending in the CO$^+$ line, as in the spectral line survey conducted toward Mon R2 (Treviño-Morales 2016) we do not find $^{13}CH_3OH$ emission at any frequency. Moreover, the main compound CH_3OH is not detected at the positions where CO$^+$ is bright.

3. Results

In Fig. 1 we compare the CO$^+$ spatial distribution with other species. Panel A shows the H^{13}CO$^+$ (3−2) line emission (black contours) tracing the molecular gas (Treviño-Morales et al. 2014), which is distributed around the CO$^+$ emission. CO$^+$ presents a clumpy structure, where the main CO$^+$ clumps seem to have a counterpart in the H^{13}CO$^+$ (3−2) emission. However, the peaks of CO$^+$ are located ≈5−10″ closer to the HII region, likely tracing an inner layer of the region. We find that CO$^+$ emission appears surrounding the HII region with its intensity peak at the offset [0″, −7″], which is very close to the IF position (see Panel B of Fig. 1). Moreover, the two most intense CO$^+$ clumps are correlated with the H_2 emission, in an area where the density is presumably larger. Panels C and D show the PAHs and the [CII] emission, respectively (black contours). The CO$^+$ emission present a clumpy ring-like distribution that is spatially coincident with the PAHs emission. The CO$^+$ secondary clumps are associated with the PAHs emission peaks, but not the most intense one. Panel D shows a comparison of the CO$^+$ spatial distribution with the emission of its chemical precursor [CII]. These species are spatially associated, with the main difference being the location of the peaks: CO$^+$ has its intensity peak to the south of the IF position, while the [CII] peak is located to the west. Therefore, we interpret that the CO$^+$ is found toward the densest area of the region (where all the molecular gas piles up, e.g., the H^{13}CO$^+$ spatial distribution) as expected since the critical densities of H^{13}CO$^+$ ($n_{cr} \sim 10^5$ cm^{-3}) and CO$^+$ ($n_{cr} \sim$ a few 10^5 cm^{-3}; Stäuber & Bruderer 2009) are larger than those of [CII] ($n_{cr} \sim$ a few 10^3 cm^{-3}; Goldsmith et al. 2012). It is worth noting that the CH$^+$ molecule is also related to the CO$^+$ and [CII] chemistry. When comparing their spatial distribution, we find that the CO$^+$ emission also coexists with CH$^+$ but, as [CII], its intensity peak is located to the west of the IF position (Pilleri et al. 2014).

In order to better understand the spatial distribution, we did intensity cuts with a position angle of 45° throughout the IF position and cut the ring-like structure seen in the CO$^+$ emission at the southeast and northwest (pink dashed line in left panel of Fig. 2). The intensity cuts for the species CO$^+$, H^{13}CO$^+$, [CII], H_2, and PAHs are shown in Panels A to F of Fig. 2. The molecular gas as traced by H^{13}CO$^+$ shows emission between the offset −20″ and 0″ (corresponding to the area between [20″, −20″] and [0″, 0″] in the map) with no emission associated with the HII region. The most intense emission of CO$^+$ comes from this region, but there is also 3σ-level emission associated with the HII region (gray-shaded area in the map). However, that the CO$^+$ peak is closer to the HII region than the H^{13}CO$^+$ peak. The [CII] emission is very intense and extended in the whole area and its intensity cut shows two emission peaks: one coincident with the CO$^+$ peak and a second peak (the brightest one) on the opposite edge of the ring-like structure (to the northwest). The PAHs emission is weaker than [CII] but their intensity cuts are very similar. Finally, the H_2 S(3) line only shows emission over 3σ between the offset −10″ and 0″. Summarizing, we can see a trend of spatial segregation with the H^{13}CO$^+$ tracing the outer layers (far from the HII region), then CO$^+$ and [CII] and PAHs peaking closer to the ionized gas and, finally, the H_2 emission tracing a hotter layer close to the HII region (Panel F of Fig. 2).

The circles in the left panel of Fig. 2 indicate the positions where we compare the spectral profiles of CO$^+$, [CII], H^{13}CO$^+$, and HCO$^+$ (Panel G). The positions correspond to (i) the ionization front (IF at offset [0″, 0″], red); (ii) the offset [−10″, 24″] (close to the PDR3 in Berné et al. 2009, black); and (iii) the MP2 position (offset [0″, 40″], blue) that is known to be a PDR with a low UV field and high density (Ginard et al. 2012). In Fig. A.1, we present a comparison of the CO$^+$ line profile (in red) with the [^{13}CII] (Ossenkopf et al. 2013), ^{13}CO (10−9), and CO (9−8) lines at IF (Pilleri et al. 2012). We find that CO$^+$ presents a larger linewidth than ^{13}CO, H^{13}CO$^+$, and HCO$^+$ (≈7 ± 0.7 km s^{-1} vs. 3−5 km s^{-1}). The CO$^+$ linewidth, however, is comparable to that of carbon recombination lines (≈6 km s^{-1}; Treviño-Morales 2016). Similarly, the CO$^+$ line has a similar profile to that of the [^{13}CII] and the high excitation CO (9−8) line. The CO$^+$ and [^{13}CII] spectra are closely similar in line shape and linewidths; this similarity may be explained well if CO$^+$ lies in the dissociation front between the ionized gas and the molecular gas. We

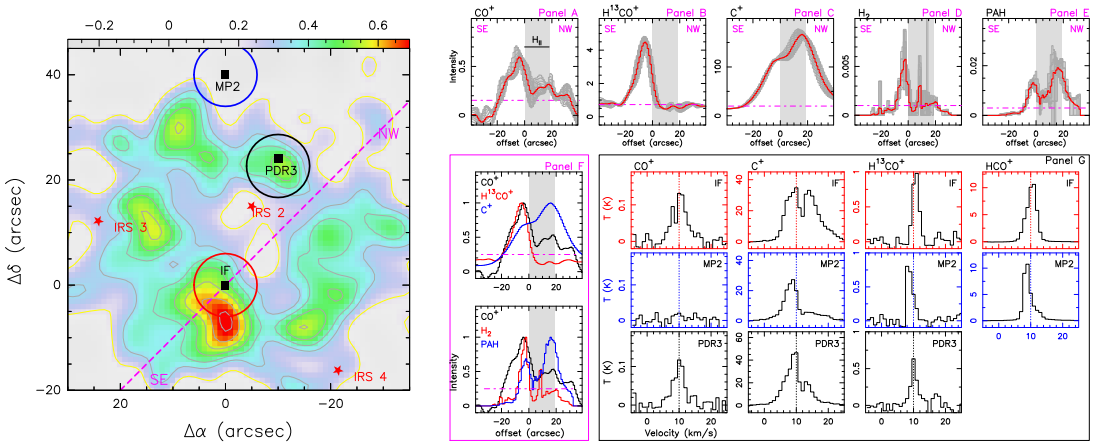

Fig. 2. *Left*: CO^+ integrated emission (see Fig. 1). The pink dashed line indicates the direction of the intensity cuts. The colored circles indicate the positions where spectra were extracted. *Right*: panel **A)** to **E)** show the intensity cuts (red continuum lines) of CO^+, $H^{13}CO^+$, [CII], H_2, and PAHs. In these panels, the gray continuum lines indicates the errors in the cuts. Panel **F)** shows the comparison of the intensity cuts scaled to unity. In panels **A)** to **F)**, the pink dot-dashed lines indicate the 3σ level for each species and the gray area indicates the position of the UC HII region. Panel **G)** shows the CO^+, [CII], $H^{13}CO^+$, and HCO^+ spectra at IF, MP2, and PDR3. The color of the boxes are related to these positions (circles in left panel).

find weak CO^+ emission toward the HII region that might come from the back and front walls of the PDR.

On the basis of reactive ions (CH^+, OH^+, and H_2O^+) observations, Pilleri et al. (2014) constructed a schematic view of the Mon R2 geometry. They find that the emission of the high density molecular gas seems to come from the back side (relative to the observer) of the HII region. This is confirmed by the detection of the cluster at infrared wavelengths (i.e., not obscured by in-front molecular gas). In this scenario, one expects that an expansion of the HII region is indicated by an excess of redshifted emission in the observed lines. However, while we find hints of the molecular tracers ($H^{13}CO^+$, CO) to be skewed toward redshifted velocities, the PDR tracers (CO^+, [^{13}CII]) seem to have a spectral profile that is skewed toward blueshifted velocities (Figs. 2 and A.1). To quantify this, we measured the amount of emission in each spectral line that is blueshifted and redshifted with respect to the systemic velocity (10 km s^{-1} for IF and PDR3, and 8 km s^{-1} for MP2; Treviño-Morales et al. 2014). For the IF position, we find 55 ± 11% of the emission of PDR tracers to be blueshifted, and only 33 ± 6% for the molecular tracers. Similarly, for MP2 and PDR3, we find 44 ± 9% and 55 ± 11% of blueshifted emission for the PDR tracers and 18 ± 4% and 39 ± 8% for the molecular tracers. In general, we have 51 ± 10% of the PDR-tracer emission to be blueshifted, and only 30 ± 6% for the molecular tracers. Considering that the molecular gas is located behind the UC HII region, the difference between the PDR and molecular tracers can be explained if the PDR is formed by dense condensations that are being photoevaporated. In this case, the photoevaporated gas (PDR tracers) would be ejected toward us, and therefore, blueshifted with respect to the molecular gas. This effect is also visible in Fig. A.1, where [^{13}CII] presents its velocity peak at ~9 km s^{-1} (blueshifted) and the emission associated with the molecular gas is redshifted. Finally, we do not find significant velocity gradients (<1 km s^{-1}) between the CO^+ clumps, suggesting low levels of turbulence between them, and this is consistent with the low expansion velocity found by Fuente et al. (2010) and Pilleri et al. (2012).

4. CO^+ and HCO^+ fractional abundances

On the basis of the spectra presented in Figs. 2 and A.1, we calculated the CO^+, HCO^+, and C^+ column density (N) in ranges of 1 km s^{-1} at the three selected positions (see Appendix B). We assume optically thin emission and a beam filling factor of 1 for all the species. The N[CO^+] values were calculated assuming a Boltzmann distribution of rotational levels with T_{ex} = 18 K. This value of the excitation temperature is based on calculations by Stäuber & Bruderer (2009) and the detection of several CO^+ lines toward the Orion Bar (Cuadrado et al. 2015, S. Cuadrado, priv. comm.). We used the MADEX large velocity gradient (LVG; Cernicharo 2012) and the RADEX code (van der Tak et al. 2007), to derive N[$H^{13}CO^+$] and N[C^+]. According to the physical conditions derived by Berné et al. (2009) from the H_2 ground-state rotational lines, we assume T_k = 600 K, n_H = 4 × 10^5 cm^{-3} for the IF and T_k = 300 K, n_H = 4 × 10^4 cm^{-3} for PDR3. Unfortunately, the MP2 position is out of the *Spitzer* map; for this position, we make a reasonable guess of T_k = 300 K and n_H = 2 × 10^5 cm^{-3}. The assumption of optically thin emission is not valid for the HCO^+ (3−2) line at velocities close to cloud systemic velocity. Thus, between 8−11 km s^{-1}, we derived the N[HCO^+] using the rarer isotopologue line $H^{13}CO^+$ (3−2) and assuming $^{12}C/^{13}C$ = 50 (Treviño-Morales et al. 2014). The derived $H^{13}CO^+$ excitation temperatures (~10−16 K) toward the IF and MP2 are in agreement with those measured by Treviño-Morales et al. (2014). The collisional rate coefficients for HCO^+ and $H^{13}CO^+$ are taken from Flower (1999). To derived the N[C^+] at the IF position, between 6−12 km s^{-1}, we used the rarer isotopologue line [^{13}CII]. A significant fraction of the [CII] emission is expected to come from the atomic layer. The calculated C^+−H collisional rates are similar to those with H_2 within a factor 1.3 (Wiesenfeld & Goldsmith 2014; Barinovs et al. 2005). Hence, the relevant parameter regarding collisional excitation is the number of particles, either H or H_2. In our calculations we assume that the hydrogen is in molecular form, which implies an uncertainty of a factor of 2 in the assumed density. Taking into account that we are well over the critical density of the [CII] 158 μm line, this translates into an uncertainty of <30% in the N[C^+]. The obtained N[C^+] are in good agreement with those obtained by Ossenkopf et al. (2013).

We computed the N[CO^+]/N[HCO^+] ratio. We found values between 0.01−0.1 toward IF with the highest values in the velocity wings. We did not detected CO^+ toward the PDR with lower UV field (MP2) with a significant upper limit of

$N[CO^+]/N[HCO^+] < 0.008$. Toward PDR3, we obtained values of $N[CO^+]/N[HCO^+] \sim 0.006$, i.e., a factor of ≈2 lower than IF. C^+ is known to be a good probe of the skin ($A_v < 4$ mag) of PDRs. Because of the similar spatial distribution and velocity profiles between the CO^+ and C^+, we used C^+ to estimate the absolute fractional abundance of CO^+. We can safely assume that almost all the carbon is in C^+ in the region from which CO^+ is coming. Assuming a carbon elemental abundance of 10^{-4} (Ossenkopf et al. 2013; Wakelam & Herbst 2008), we derive $X[CO^+]$ between a few 10^{-11} to $\sim 1.9\times10^{-10}$ toward both IF and PDR3. The beam of CO^+, HCO^+, $H^{13}CO^+$, [^{13}CII], and [CII] are very similar, thus the calculated $N[CO^+]/N[HCO^+]$, and $X[CO^+]$ values are not affected by beam filling factors. Our results are in good agreement with the model predictions presented by Sternberg & Dalgarno (1995) for $G_0 \sim 5 \times 10^5$ and $n_H \sim 10^6$ cm^{-3}. More recently, the models of Spaans & Meijerink (2007) predict the $X[CO^+]$ in PDRs for $n_H = 10^5$ cm^{-3} and $G_0 = 10^{3.5}$. However, the high cosmic ray ionization rate (about 100 times larger than the Galactic value) prevents us from a direct comparison with Mon R2. In general, the production of CO^+ seems to depend on the temperature of the gas. Stäuber & Bruderer (2009) suggest that $X[CO^+]$ of about 10^{-11} are only reached in gas with $T_k \geq 300$ K. As T_k depends on G_0 and n_H, it is expected that the production of CO^+ only occurs in regions with $n_H \geq 2 \times 10^4$ cm^{-3} and $G_0 \geq 10^3$. The densities and G_0 measured in IF and PDR 3 are in good agreement with these values, as IF presents $G_0 \sim 5 \times 10^5$ and $n_H \geq 5 \times 10^4$ cm^{-3} (Rizzo et al. 2003; Fuente et al. 2010) and PDR3 presents $G_0 \sim 3.7 \times 10^4$ and $n_H \sim 3.7 \times 10^4$ cm^{-3} (Berné et al. 2009).

5. Discussion and summary

We present a CO^+ map toward the Mon R2 star-forming region. This is the first map ever reported of this reactive ion. The spatial distribution of CO^+ consists of a ring-like structure (similar to PAHs), tracing the layer between the HII region and the molecular gas. The maps reveal a clumpy structure in the hot layer of the mainly atomic gas. Previous works (Young et al. 2000; Goicoechea et al. 2016) suggest that fragmentation exists in the photodissociation front. As such, uniform layers do not exist between the HII region and the molecular cloud, but they present clumps that allow the radiation to penetrate deeper into the cloud. In this scenario, where the PDR is conformed by a series of clumps, the emission of PDR tracers would be related to the external layers of dense clumps that are photoevaporated by the UV radiation. Despite the moderate angular resolution of our observations, we find hints that favor this scenario: first, the spatial distribution of the CO^+ as observed in the higher angular resolution (11″) map (Panel A of Fig. 1) suggests that the CO^+ emission is coming from the illuminated surface of the $H^{13}CO^+$ clumps, and, second, the excess of blueshifted emission seen for the PDR tracers in comparison with the molecular tracers. Considering that the molecular gas is located behind the UC HII region (Pilleri et al. 2014) and the chemical segregation, the difference in velocity between tracers can be explained if the PDR is formed by dense condensations that are being photoevaporated. In this case, the photoevaporated gas (PDR tracers) would be ejected toward us, and therefore, blueshifted with respect to the molecular gas. Future higher angular resolution observations will help to confirm or discard this scenario.

Finally, we determined $X[CO^+]$ in three positions. We derive an abundance of a few 10^{-11} toward IF, which is in agreement with chemical model predictions (Sternberg & Dalgarno 1995) for $n_H \sim 10^6$ cm^{-3} and $G_0 \sim 5 \times 10^5$. We do not detect CO^+ emission with an upper limit to the CO^+ abundance of $<4 \times 10^{-11}$ toward MP2. Abundances of 10^{-11}–10^{-10} had been previously observed in PDRs with $G_0 > 10^3$ Habing field (M17SW: Latter et al. 1993, Stoerzer et al. 1995; Orion Bar: Fuente & Martín-Pintado 1997; NGC 7023: Fuente et al. 2003; G29.96−0.02: Rizzo et al. 2003). The nondetection of CO^+ in MP2, together with the abundances found in the other PDRs, suggest that the production of CO^+ only occurs in dense regions with high radiation fields. High UV fields ($G_0 > 10^3$) and n_H ($>2\times10^4$ cm^{-3}) are required to achieve gas temperatures ≥300 K, which are necessary to produce high abundances of OH in the external layer of the PDR ($A_V \sim 1$ mag; Stäuber & Bruderer 2009). This is also consistent with the nondetection of CO^+ in the Horsehead PDR (Goicoechea et al. 2009), where the UV field is $G_0 \sim 100$ and presents chemical properties similar to MP2 (Ginard et al. 2012). A counterexample that challenge this interpretation could be the detection of CO^+ toward S140, where the incident UV field is estimated to be $G_0 \sim 100$–300 (Savage & Ziurys 2004). However, the number of CO^+ detections is scarce and the statistics is not enough to draw firm conclusions between the relation of the CO^+ and the physical properties (n_H and G_0) of PDRs. A larger sample of objects need to be studied, including maps to characterize and understand the spatial distribution of the CO^+ in different environments.

Acknowledgements. S.P.T.M., A.F., J.R.G. and J.C., thank the Spanish MINECO for funding support from grants AYA2012-32032, CSD2009-00038, FIS2012-32096, and ERC under ERC-2013-SyG, G. A. 610256 NANOCOSMOS. A.S.M. and V.O. thank the Deutsche Forschungsgemeinschaft (DFG) for funding support via the collaborative research grant SFB 956, projects A6 and C1. P.P. acknowledges financial support from the Center National d'Études Spatiales (CNES).

References

Barinovs, Ğ., van Hemert, M. C., Krems, R., & Dalgarno, A. 2005, ApJ, 620, 537
Berné, O., Fuente, A., Goicoechea, J. R., et al. 2009, ApJ, 706, L160
Cernicharo, J. 2012, in EAS Pub. Ser., 58, 251
Cuadrado, S., Goicoechea, J. R., Pilleri, P., et al. 2015, A&A, 575, A82
Flower D. R. 1999, MNRAS, 305, 651
Fuente, A., & Martín-Pintado, J. 1997, ApJ, 477, L107
Fuente, A., Rodrıguez-Franco, A., Garcıa-Burillo, S., et al. 2003, A&A, 406, 899
Fuente, A., Berné, O., Cernicharo, J., et al. 2010, A&A, 521, L23
Ginard, D., González-García, M., Fuente, A., et al. 2012, A&A, 543, A27
Goicoechea, J. R., Pety, J., Gerin, M., et al. 2009, A&A, 498, 771
Goicoechea, J. R., Pety, J., Cuadrado, S., et al. 2016 Nature, DOI: 10.1038/nature18957
Goldsmith, P. F., Langer, W. D., et al. 2012, ApJS, 203, 13
Habing, H. J. 1968, Bull. Astron. Inst. Netherlands, 20, 120
Herbst, W., & Racine, R. 1976, AJ, 81, 840
Latter, W. B., Walker, C. K., & Maloney, P. R. 1993, ApJ, 419, L97
Ossenkopf, V., Röllig, M., Neufeld, D. A., et al. 2013, A&A, 550, A57
Pety, J., Teyssier, D., Fossé, D., et al. 2005, A&A, 435, 885
Pilleri, P., Fuente, A., Cernicharo, J., et al. 2012, A&A, 544, A110
Pilleri, P., Treviño-Morales, S., Fuente, A., et al. 2013, A&A, 554, A87
Pilleri, P., Fuente, A., Gerin, M., et al. 2014, A&A, 561, A69
Rizzo, J. R., Fuente, A., Rodrıguez-Franco, A., & Garcıa-Burillo, S. 2003, ApJ, 597, L153
Savage, C., & Ziurys, L. M. 2004, ApJ, 616, 966
Spaans, M., & Meijerink, R. 2007, ApJ, 664, L23
Stäuber, P., & Bruderer, S. 2009, A&A, 505, 195
Sternberg, A., & Dalgarno, A. 1995, ApJS, 99, 565
Stoerzer, H., Stutzki, J., & Sternberg, A. 1995, A&A, 296, L9
Treviño-Morales, S. P. 2016, Ph.D. Thesis
Treviño-Morales, S. P., Pilleri, P., Fuente, A., et al. 2014, A&A, 569, A19
van der Tak, F. F. S., Black, J. H., Schöier, F. L., et al. 2007, A&A, 468, 627
Wakelam, V., & Herbst, E. 2008, ApJ, 680, 371
Wiesenfeld, L., & Goldsmith, P. F. 2014, ApJ, 780, 183
Young Owl, R. C., Rolaine, C., Meixner, M. M., et al. 2000, ApJ, 540, 886

Appendix A: Comparison with other lines

In this section we present the comparison of the CO^+, [^{13}CII], ^{13}CO (10−9), and CO (9−8) line profiles. Figure A.1 shows the CO^+ (in red), [^{13}CII] (Ossenkopf et al. 2013), ^{13}CO (10−9), and CO (9−8) lines (in black) at the IF position (Pilleri et al. 2012) with the intensity is scaled to unity. We find that CO^+ presents a larger linewidth than ^{13}CO and $H^{13}CO^+$ (≈7 ± 0.7 km s^{-1} vs. 3−5 km s^{-1}). Moreover, the CO^+ line has a similar profile to that of the [^{13}CII] and CO line. The [^{13}CII] line presents its velocity peak at ∼9 km s^{-1}and the emission associated with the molecular gas (CO, ^{13}CO) is redshifted, while the systemic velocity is ∼10 km s^{-1}.

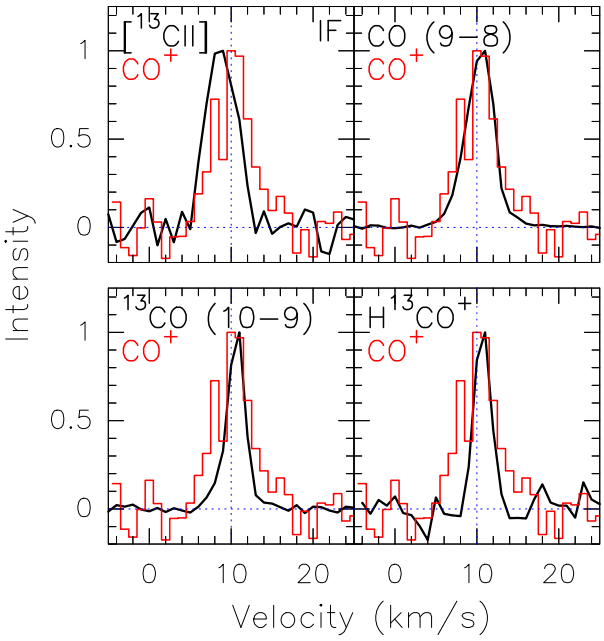

Fig. A.1. Comparison of the CO^+ line profile (in red) with the [^{13}CII], ^{13}CO (10−9), CO (9−8), and $H^{13}CO^+$ lines (in black) at the IF position, where the intensity is scaled to unity. *Herschel* data are presented in Pilleri et al. (2012) and Ossenkopf et al. (2013). The blue dotted line indicates the systemic velocity (10 km s^{-1}).

Appendix B: Column densities and fractional abundances

In this section we present the calculated CO^+, HCO^+, and C^+ column densities (N), as well as the fractional abundance $X(CO^+)$ of the IF, MP2, and PDR3 positions. The column densities were calculated in ranges of 1 km s^{-1} from 5 km s^{-1} to 14 km s^{-1}. The CO^+ column densities have been calculated assuming a Boltzmann distribution of rotational levels with T_{ex} = 18 K. While for HCO^+ and C^+, we used RADEX and MADEX LVG codes (van der Tak et al. 2007; Cernicharo 2012), considering the physical conditions derived by Berné et al. (2009). For the IF position, the HCO^+ emission is optically thick and, thus, we used the rarer isotopologue $H^{13}CO^+$ to correct the opacity effects and derive $N[HCO^+]$ in each position, assuming $^{12}C/^{13}C$ = 50 (Treviño-Morales et al. 2014). Regarding the $N[C^+]$ estimation, we note that [CII] is optically thick toward the IF position (as seen by comparing the [CII] and [^{13}CII] lines); under the assumption of optically thin emission, [^{13}CII] results in a column density a factor 3−5 larger than that derived from the main isotopologue [CII]. From this, and considering that the other two positions are associated with less dense gas, we can infer that the assumption of optically thin emission applied to the [CII] in MP2 and PDR3, may underestimate the column density by a factor <3. Because of the similar spatial distribution and velocity profiles between the CO^+ and C^+, we used $N[C^+]$ to estimate the absolute fractional abundance $X(CO^+)$. For the calculations, we consider a beam filling factor of 1. This assumption is consistent with the fact that the beams of [CII] at 158 μm, $H^{13}CO^+$ (3−2), HCO^+ (3−2), and CO^+ (2−1) are very similar. Thus the calculated $N[CO^+]/N[HCO^+]$ and $X[CO^+]$ values are not affected by the beam filling factor. Table B.1 lists the calculated values of $N[CO^+]$, $X[CO^+]$, $N[HCO^+]$, $N[C^+]$, and $N[CO^+]/N[HCO^+]$ in every velocity range.

Table B.1. Column densities and ratios, in ranges of 1 km s^{-1}, of the selected positions (see Fig. 2).

Velocity range	(km s^{-1})	5−6	6−7	7−8	8−9	9−10	10−11	11−12	12−13	13−14	Total*
For the CO$^+$ line		∼3σ				>3σ				∼3σ	
IF position — offset [0″, 0″]											
N[CO$^+$]	(in 10^{11} cm^{-2})	0.14	0.50	1.34	1.34	1.20	1.90	1.60	0.82	0.57	9.75[a]
N[HCO$^+$]	(in 10^{13} cm^{-2})	<0.04	0.06	0.15	0.34	1.44	2.42	1.92	0.70	0.05	6.79[a]
N[C$^+$]	(in 10^{17} cm^{-2})	0.63	4.00	5.10	6.00	5.60	4.70	3.30	1.24	1.67	48.00[b]
N[CO$^+$]/N[HCO$^+$]		>0.04	0.08	0.09	0.04	0.08	0.08	0.01	0.01	0.11	0.02
X[CO$^+$]	(in 10^{-11})	2.22	1.47	2.16	2.23	2.14	4.04	4.90	6.61	3.41	2.03
MP2 position — offset [0″, 40″]											
N[CO$^+$]	(in 10^{11} cm^{-2})	<1.71	<1.71	<1.71	<1.71	<1.71	<1.71	<1.71	<1.71	<1.71	<4.5[d]
N[HCO$^+$]	(in 10^{13} cm^{-2})	<0.04	0.06	0.29	2.21	1.46	0.71	0.29	0.06	0.06	5.84[a]
N[C$^+$]	(in 10^{17} cm^{-2})	0.63	0.97	1.31	1.52	1.38	0.78	0.34	0.29	0.33	10.15[c]
N[CO$^+$]/N[HCO$^+$]		>0.043	<0.285	<0.058	<0.007	<0.011	<0.024	<0.058	<0.29	<0.285	<0.008
X[CO$^+$]	(in 10^{-10})	<2.71	<1.76	<1.31	<1.13	<1.24	<2.19	<5.03	<5.89	<5.18	<0.45
PDR3 position — offset [−10″, 24″]											
N[CO$^+$]	(in 10^{11} cm^{-2})	<1.35	0.58	1.19	1.77	2.45	2.68	1.66	0.72	<1.35	13.02[a]
N[HCO$^+$]	(in 10^{13} cm^{-2})	<3.34	<3.34	<3.34	1.70	5.17	6.10	3.04	<3.34	<3.34	20.22[a]
N[C$^+$]	(in 10^{17} cm^{-2})	0.99	1.37	1.68	2.26	2.70	1.93	0.95	1.00	1.14	18.04[c]
N[CO$^+$]/N[HCO$^+$]		>0.004	>0.002	>0.004	0.010	0.005	0.004	0.005	>0.002	>0.004	0.006
X[CO$^+$]	(in 10^{-10})	1.36	0.42	0.71	0.78	0.91	1.92	1.75	0.72	1.18	0.72

Notes. We assumed LTE and T_{ex} = 18 K to calculate N[CO$^+$], while N[HCO$^+$] and N[C$^+$] were calculated assuming LVG. For the IF position, we assume T_k = 600 K, $n_H = 4 \times 10^5$ cm^{-3}. For MP2 position, we assume T_k = 300 K and $n_H = 2 \times 10^5$ cm^{-3}. For PDR3 position, we assume T_k = 300 K and $n_H = 4 \times 10^4$ cm^{-3}. (*) Total velocity range of each line. [(a)] In a velocity range of 5−14 km s^{-1}. [(b)] In a velocity range of 4−25 km s^{-1}. [(c)] In a velocity range of 0−30 km s^{-1}. [(d)] considering the rms in a velocity range of 7 km s^{-1}.